ГИАБ. Горный информационно-аналитический бюллетень /
MIAB. Mining Informational and Analytical Bulletin, 2023;(4):107-124
ОРИГИНАЛЬНАЯ СТАТЬЯ / ORIGINAL PAPER

УДК 552.1+531/534 DOI: 10.25018/0236_1493_2023_4_0_107

ПРОГНОЗ ОБРАЗОВАНИЯ ВЗВЕШЕННОЙ АЭРОЗОЛЬНОЙ УГОЛЬНОЙ ПЫЛИ ПРИ МЕХАНИЧЕСКИХ ВОЗДЕЙСТВИЯХ. Часть 1. ВЛИЯНИЕ СТРУКТУРЫ УГЛЕЙ РАЗНОЙ СТАДИИ МЕТАМОРФИЗМА НА МЕХАНИЧЕСКОЕ ПОВЕДЕНИЕ ПРИ ЦИКЛИЧЕСКОМ НАГРУЖЕНИИ

С.А. Эпштейн[1], Е.Л. Коссович[1], М.Г. Минин[1], Н.Н. Добрякова[1], Д.И. Гаврилова[1]

[1] НИТУ «МИСиС», Москва, Россия, e-mail: e.kossovich@misis.ru

Аннотация: Проведено исследование механических свойств углей на микроуровне и характера их разрушения при циклическом нагружении. Прочность углей в целом увеличивается с увеличением стадии метаморфизма. Для рассмотренных образцов углей после экспериментов по циклическому наноиндентированию и оценки нового параметра $E_{compaction}$ были выявлены три основных характера разрушения: «локальный», «в объеме» и «переходная зона». Отнесение углей к группам в соответствии с характером разрушения не определяется стадией метаморфизма. Однако параметр $E_{compaction}$ линейно увеличивается с ростом отношения доли аморфного углерода к кристаллитному (параметр S), рассчитанного с использованием рамановской спектроскопии. «Переключение» между группами происходит, когда S достигает 1. Таким образом, угли из группы «локальное разрушение» характеризуются преобладанием кристаллического углерода в веществе витринита, угли из группы «разрушение в объеме» – это угли с преобладанием аморфного углерода. Угли из группы «переходная зона» характеризуются равным соотношением аморфного и кристаллитного углерода в витрините.

Ключевые слова: уголь, антрацит, метаантрацит, стадия метаморфизма, разрушение, циклическое наноиндентирование, Рамановская спектроскопия, аморфные соединения углерода, кристаллитные соединения углерода.

Благодарность: Работа выполнена при поддержке Программы стратегического академического лидерства «Приоритет 2030».

Для цитирования: *Эпштейн С. А., Коссович Е. Л., Минин М. Г., Добрякова Н. Н., Гаврилова Д. И.* Прогноз образования взвешенной аэрозольной угольной пыли при механических воздействиях. Часть 1. Влияние структуры углей разной стадии метаморфизма на механическое поведение при циклическом нагружении // Горный информационно-аналитический бюллетень. – 2023. – № 4. – С. 107–124. DOI: 10.25018/0236_1493_2023_4_0_107.

Prognosis of fine airborne coal dust formation at mechanical effects. Part 1. Effects of structure of different rank coals at their mechanical behavior at cyclic loading

S.A. Epshtein[1], E.L. Kossovich[1], M.G. Minin[1], N.N. Dobryakova[1], D.I. Gavrilova[1]

[1] National University of Science and Technology «MISiS», Moscow, Russia,
e-mail: e.kossovich@misis.ru

Abstract: An investigation has been performed aimed at characterization of coals mechanical properties at micro scale and modes of their crushing under cyclic loading. Strength of coals generally increases with rank. Three principal types of s crushing mode have been revealed for the considered range of coals' samples tested by means of cyclic nanoindentation and evaluation of new $E_{compaction}$ parameter; «local», «bulk» and «transition zone». Attribution of coals to groups in accordance with the crushing mode does not depend on their rank. But, $E_{compaction}$ parameter linearly increases with the amorphous-to-crystalline carbon ratio (parameter S) calculated with help of Raman spectroscopy. The 'switching' between the crushing modes occurs when S reaches 1 sharp. Thus, coals from the «local crushing» group are characterized by crystalline carbon predomination in vitrinite matter, «bulk crushing» group of coals are those with amorphous carbon predomination. The coals from «transition group» have been characterized by equal share of amorphous and crystalline carbon in their vitrinites.

Key words: coal, anthracite, metaanthracite, rank, crushing, cyclic nanoindentation, Raman spectroscopy, amorphous carbon, crystalline carbon.

Acknowledgements: The research has been financially supported by the Program of strategic academic leadership «Priority 2030».

For citation: Epshtein S. A., Kossovich E. L., Minin M. G., Dobryakova N. N., Gavrilova D. I. Prognosis of fine airborne coal dust formation at mechanical effects. Part 1. Effects of structure of different rank coals at their mechanical behavior at cyclic loading. *MIAB. Mining Inf. Anal. Bull.* 2023;(4):107-124. [In Russ]. DOI: 10.25018/0236_1493_2023_4_0_107.

Introduction

Coal dust emission is one of the most hazardous processes that occur at coal mining and processing industries. It is widely known that fine airborne coal dust is able to be dispersed in air and stay there for a considerably long time terms [1, 2]. This feature of airborne coal dust reasons for its inhaling by the workers, and, consequently, leads to formation and development of different dangerous health damages [3–5]. Also, when dispersed in air, the fine airborne coal dust is able to be transported with air flows at considerable distances with further settling at soils and waters and serving as a hazardous pollutant (including hazardous microelements) [1, 5, 6]. Coal dust is no less dangerous in terms of potentially dangerous gas-dynamic phenomena (explosions) [2, 7].

In a view of above, the issues of coals' propensity to fine airborne dust formation are relevant. Traditionally, coals' propensity to fine airborne dust formation is associated with their mechanical properties and proneness to crushing under external effects. Initially, the relevant studies were dedicated to finding the principle mecha-

nical properties of coals that may affect the dust formation processes during coals extraction. This included hardness, density and porosity of coal matter [8], average compressive strength [9], Hardgrove grindability [10—12], etc. Tight connection of the latter with the amount of releasing airborne dust allowed the researchers to look for some features of coals' structure that are responsible for high or low proneness to fine dust release at mechanical impacts. These features included rank [10, 13, 14] and maceral composition [10, 13, 15]. Although petrographic composition of coals was proved to have some effects on their proneness to fine dust formation, the data is rather controversial (for more details, see [10, 13, 15] indicating on different types of macerals and microlitotypes that are responsible for airborne dust generation). It mostly determines the grindability and amount of fine classes of particles, but not fine enough to be related to airborne dust. On the other hand, the amount of airborne dust formed during coal crushing has an increasing trend with coal rank [16—18], although with a rather high distortion of data for the range of middle-rank bituminous coals [16].

Modern ideas on interconnections between coals mechanical properties and their propensity to crushing with fine airborne dust formation are based on the assumption that the defects initiation and growth occurs firstly at nano- and microscales [19, 20]. Therefore, the mechanical properties of coals should be studied at the corresponding scales. Based on these assumptions, independently, authors of [21, 22] have proposed that micro- and nanoindentation of coals as brittle materials leads to their destruction in the contact zone with formation of a core of finely crushed material. Processes of airborne coal dust formation at coal crushing were preliminarily studied by means of cyclic nanoindentation [23, 24].

In the view of above, the aim of the current paper is to establish the interconnections between coals mechanical properties at low scales and their crushing features (modes) that lead to fine airborne dust formation during external mechanical effects at them (e.g. during mining or transshipment).

Materials and methods

Coals samples

For experiments, 17 hard coals from Kuznetsk and Pechora coal basins and four anthracites from Donetsk and Gorlovsky coal basins and Omsukchansk coal field were used. Characteristics of coals are presented in Table 1. In addition, metaanthracite was used originating from the same coal coal field (Omsukchansk).

The sample set is represented by 17 hard coals with a wide range of vitrinite reflectance (from 0.56 up to 1.89%). In general, coals' petrographic composition is represented by prevalence of vitrinite contents. The exception is coals #830 and 825 that are characterized by prevailing of inertinite (58 and 64% Vol., respectively). Anthracites #857 and 871 are characterized by the close petrographic composition and vitrinite reflectance (the highest in the range of anthracites and metaanthracite ##1, 2, 10, 857 and 871). Anthracite #10 and has considerably higher rank in comparison with metaanthracite #2.

In order to carry out the experiments on nanoindentation and Raman spectroscopy, the particulate blocks of run-of mine coals were prepared similar to ISO 7404-2:2009. To this end the samples were used as described in section 2.2. An epoxy resin was used as a binder providing the lack of intrusion of it into the coal grains.

Tests on nanoindentation and Raman spectroscopy were carried out on vitrinite as on maceral, which is the most susceptible to changes in mechanical properties with increasing rank [25].

Table 1

Characteristics of coals
Характеристики углей

#	Coal type	Origin	Petrographic composition, % Vol.			*Ro.r*, % (vitrinite reflectance index)
			Vt (vitrinite)	I (intertinite)	L (liptinite)	
824	hard coal	Kuznetsk basin	61	36	4	0.56
827	hard coal	Kuznetsk basin	75	22	3	0.61
829	hard coal	Kuznetsk basin	68	28	4	0.61
4**	hard coal	Kuznetsk basin	70	20	10	0.65
873	hard coal	Kuznetsk basin	75	23	2	0.85
580	hard coal	Pechora basin	91	7	2	0.89
581	hard coal	pechora basin, pack potentially prone to sudden outbursts	86	13	1	0.92
518	hard coal	Kuznetsk basin	56	42	2	0.95
830	hard coal	Kuznetsk basin	41	58	1	1
828	hard coal	Kuznetsk basin	49	51	0	1.05
826	hard coal	Kuznetsk basin	63	35	2	1.09
822	hard coal	Kuznetsk basin	52	48	0	1.11
517	hard coal	Kuznetsk basin	48	52	0	1.13
825	hard coal	Kuznetsk basin	36	64	0	1.15
516	hard coal	Kuznetsk basin	67	33	0,0	1.65
839	hard coal	Kuznetsk basin	69	31	0	1.7
823	hard coal	Kuznetsk basin	65	35	0	1.89
1	anthracite	Omsukchansk coalfield	n/d*	n/d	n/d	2.57
2	metaanthracite	Omsukchansk coalfield	n/d	n/d	n/d	3.28
10	anthracite	Donetsk basin	91,0	9,0	0	3.58
857	anthracite	Gorlovsky basin	68	32	0	4.14
871	anthracite	Gorlovsky basin	67	33	0	4.25

*n/d – not determined
** Italic font denotes the coals that have been used in the sample set in paper [24].

Nanoindentation experiments

Experiments were held at Hysitron TI 750 UBI nanotriboindenter with a built-in surface analyzer (scanning probe microscopy) and TriboScan software for automated experimentation and data processing.

Nanoindentation was performed at the surfaces occupied by vitrinite and characterized by optical uniformity and absence of a pronounced relief and defects. The roughness of the selected sites determined by scanning probe microscopy did not exceed 0.5 μm.

Two types of nanoindentation experiments were applied. Quasi-static nanoindentation experiments were carried out on

selected sites (at least two for each of the samples) by grid technique In total, at least 36 indentations were carried out on each of the selected sites. The value of the maximum load was selected individually for each of the coals in accordance with the method described in [19]. A trapezoidal protocol was used as a loading scheme: 5 seconds — loading to the maximum value, 2 seconds — exposure under maximum load, 5 seconds — unloading (at a speed corresponding to the loading one).

The results of these experiments included:

• contact modulus of elasticity *E*, determined in accordance with the Bulychev-Alekhin-Shorshorov dependence [26] by the slope of the initial part of the unloading branch;

• damage index, *Rw*. It characterizes the ability of a brittle material to fracture. Its choice is due to the fact that it was previously established that coals are a brittle material that can be crushed under low loading values (during nanoindentation) [22]. The damage index is determined based on the ratio of the hysteresis loop area of the loading-unloading curve, which is being built automatically by the nanohardness equipment, to the total work of the forces on loading the sample [27].

Cyclic nanoindentation experiments were performed in accordance with the previously developed technique [28]. A twelve-stage cyclic loading mode was chosen, with the peak loading value increasing exponentially from 0.01 to 12 mN. The loading protocol for each cycle was similar to the one used in quasi-static experiments. The graphical representation of the loading mode is given in Fig. 1. The cycles numbers and the corresponding peak load are shown in Table 2.

Table 2

Assignment of cycles number and peak load P_{max}
Соотнесение номера цикла нагружения и величины максимальной нагрузки P_{max}

Cycle #	P_{max}, μN
1	10
2	170
3	500
4	1000
5	1700
6	2600
7	3700
8	5000
9	6400
10	8100
11	10 000
12	12 000

The results of the cyclic nanoindentation were processed in accordance with the approach shown in [24, 29]. That is,

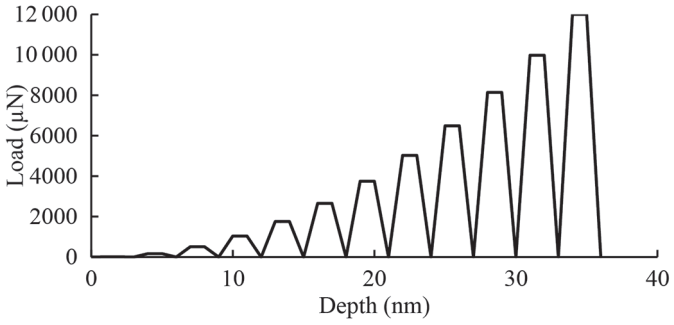

Fig. 1. Loading mode for the cyclic nanoindentation experiments
Рис. 1. Режим нагружения при экспериментах по циклическому наноиндентированию

for each of the samples, a set of data was obtained on the values of the modulus of elasticity and the damage index for eight separate cyclic loadings performed at different zones occupied by vitrinite. The data were averaged separately for each cycle, and the standard deviation of the values was also calculated (it did not exceed 5% of the average for both the elastic moduli and the damage indices).

In the current paper, only the numerical data has been further discussed. It included the values of the elastic modulus obtained by quasistatic nanoindentation (E) and cyclic indentation after the tenth cycle of loading (*E10*), as well as the corresponding damage indices *Rw* (after quasistatic loading) and *Rw10* (after ten cycles of nanoindentation).

In order to establish the influence of the mechanical properties of coals on the content of fine airborne dust in them, the parameter $E_{\text{compaction}}$ was calculated [23, 24].

$$E_{compaction} = \frac{E - E10}{E} * 100\% \qquad (1)$$

This parameter reflects the degree of compaction of the coal under the indenter during cyclic loading with increasing maximum load. In this case, compaction of the coal matter occurs if *E10* index exceeds the elastic modulus measured during quasi-static nanoindentation.

Raman spectrocopy

Raman spectroscopy measurements were carried out to investigate the structural features of the coal samples vitrinite. To this end, EnSpectr R532 Raman spectrometer mounted on Olympus BX 51 microscope was used. The spectrometer is operating with a universal green 532 nm lazer with resolution of 4 cm^{-1}. The laser power was set up to 5 mW (depending on the coal sample under study), integration time was 2 s. Measurements were performed at the petrographic samples' surface occupied with optically homogenous vitrinite in air at a room temperature. Not less than 30 measurements (each at different zone occupied by vitrinite) were performed at each sample. Further, the spectral data for each of the coal was processed to obtain the smooth spectra in the range of Raman shift of 1000 — 1800 cm^{-1}.

The structural features of vitrinite were studied on the basis of the wide bands D and G deconvolution into the narrower

Table 3

Characteristics of the peaks for fitting the coals Raman spectroscopy data (for more details see [24, 30–32])
Характеристики пиков для деконволюции Рамановских спектров углей (подробнее см. [24, 30—32])

Name of the peak	Approximate position, cm^{-1} (Raman shift)	Characteristics	Carbon compounds type
SL	1230	volatile hydrocarbon compounds, polyenes	amorphous
D	1370	graphite lattice defects, graphite edge defects	crystalline
VR	1380	methyl groups	amorphous
VL	1460	methylene groups	amorphous
GR	1540	amorphous carbon, aromatics with less than 5 rings	amorphous
G	1580	perfect graphitic structures	crystalline
G2	1600	disordered graphitic structures, surface graphitic layers	crystalline

ones representing different carbon compounds. The model of peaks fitting used in this work well correlates with the ones previously discussed in [30–32]. It consists of seven bands fitted by the Lorenzian-type peaks. The assignment of the bands to carbon compounds is listed in Table 3. Their attribution to crystalline and amorphous types of carbon compounds is based on the discussion in [30] and subsequent works on coal Raman spectra interpretation.

According to [24], a new parameter has been used based on the aforementioned Raman bands deconvolution. It is the ratio of amorphous to crystalline carbon compounds in vitrinite. The areas (*A*) of the peaks of the corresponding bands are used. The sum of areas of peaks assigned to the amorphous form of carbon ($S_{amorphous}$) is calculated by eq. (2).

$$S_{amorphous} = A\,SL + A\,VR + A\,VL + A\,GR\,. \quad (2)$$

And the sum of areas of peaks assigned to crystalline form of carbon ($S_{crystal}$) by eq. (3).

$$S_{crystal} = A\,D + A\,G + A\,G2\,. \quad (3)$$

Then, the ratio of amorphous to crystalline carbon compounds in coal vitrinite is found by eq. (4).

$$S = \frac{S_{amorphous}}{S_{crystal}}\,. \quad (4)$$

Statistical analysis of the results revealed the error of *S* parameter evaluation not exceeding 0.5%.

Results and Discussion

The results of measurements of the mechanical properties of coals' vitrinites at microscale by quasi-static and cyclic nanoindentation are presented in Table 4.

Coals differ in the value of the modulus of elasticity. Its highest values are noted for anthracites. For hard coals, their elastic moduli are in general increasing with rank, but with high degree of distortion (Fig. 2). *E10* values differ from those measured by quasi-static nanoindentation, namely, for some coals they increase, for some – decrease, and there are several cases when they do not change.

It is interesting to note that the shape of the P-h curve is variant with respect to the coal rank (see Fig. 3). Indeed, it could

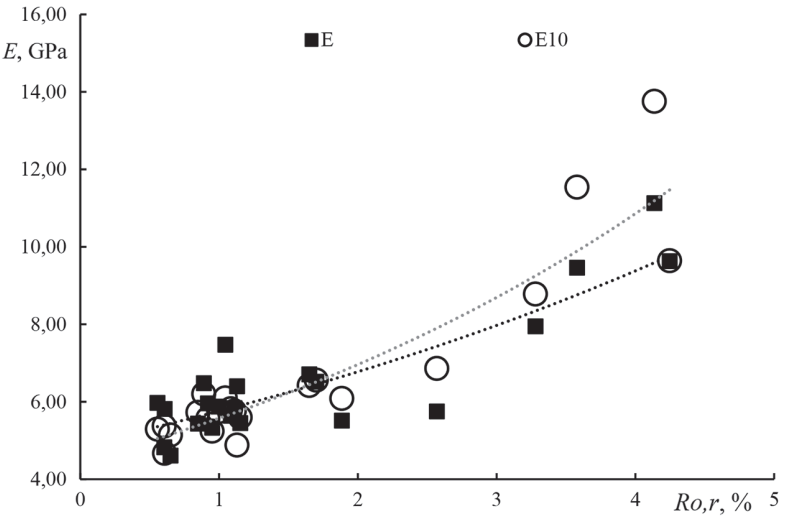

Fig. 2. The relationship between the values of the modulus of elasticity of coals and their rank
Рис. 2. Взаимосвязь между модулями упругости углей и их стадией метаморфизма

Table 4

Mechanical properties of vitrinites of coals determined by the methods of cyclic and quasi-static nanoindentation

Механические свойства витринитов углей, определенные методами циклическогои квази-статического наноиндентирования

Sample #	Quasi-static nanoindentation				Cyclic nanoindentation				$E_{compaction}$, %
	E, GPa	StDev* *E*, GPa	*Rw*, %	StDev* *Rw*, %	*E10*, GPa	StDev* *E10*, GPa	*Rw10*, %	StDev* *Rw10*, %	
4**	4,61	0,08	33	1	5.14	0.01	29	2	–11,41
580	6,48	0,18	40	2	6.20	0.06	26	2	4,29
581	5,96	0,22	41	5	5.57	0.10	30	4	6,61
518	5,33	0,26	32	2	5.24	0.09	24	3	1,65
517	6,40	0,21	28	4	4.88	0.02	24	3	0,49
516	6,71	0,29	28	2	6.42	0.12	18	1	4,38
1	5,75	0,69	17	4	6.86	0.15	11	3	–19,27
2	7,95	0,11	11	1	8.78	0.16	9	1	–10,52
10	9,46	0,11	9	0	11.54	0.01	6	0	–22,01
822	5.84	0.64	41	6	5.76	0.24	25	3	1.31
823	5.51	0.35	30	3	6.08	0.23	28	2	–10.34
824	5.97	0.31	42	3	5.29	0.29	29	1	11.40
825	5.45	0.13	30	1	5.60	0.30	22	1	–2.72
826	5.64	0.38	32	3	5.82	0.21	25	1	–3.23
827	4.83	0.64	43	2	5.37	0.21	29	1	–11.37
828	7.47	1.46	38	9	6.10	0.23	28	4	18.40
829	5.82	0.14	43	2	4.67	0.27	36	6	19.74
830	5.88	0.57	34	4	5.75	0.27	21	1	2.21
839	6.52	0.73	37	10	6.56	0.91	27	6	–0.60
857	11.13	0.62	10	1	13.76	0.49	8	4	–23.61
871	9.63	0.37	10	3	9.64	0.37	9	1	–0.12
873	5.44	0.11	35	1	5.73	0.08	26	3	–5.32

* StDev – a standard deviation of the corresponding value.

** italic font denotes the coals that has been used previously in paper [24].

be seen that the higher the vitrinite reflectance, the more the shape of P-h curve tends to the elastic one. The qualitative jump from elasto-plastic shapes with a pronounced hysteresis loop to the almost elastic one is found for anthracites. Such an observation supports data shown in Fig. 3 on the variation of the damage index *Rw* with rank.

Table 4 shows that the damage indices *Rw10* measured after the tenth loading cycle are lower than those obtained by a single (quasi-static) nanoindentation *Rw*. This indicates on some compaction of the coal matter under cyclic mechanical impacts with an increasing maximum load [24]. The general descend of the damage indices with rank growth was observed

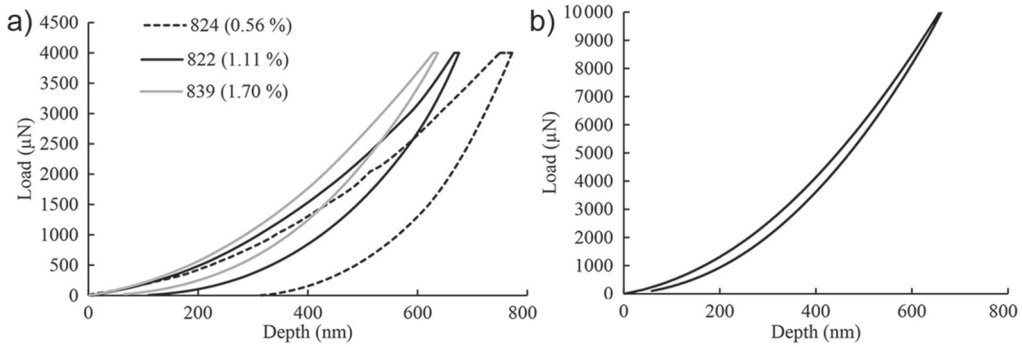

Fig. 3. An example of P-h curves obtained after quasi-static nanoindentation of coals of different rank: hard coals of low ($R_{o,r}$ = 0.56%), medium ($R_{o,r}$ = 1.11%) and high ($R_{o,r}$ = 1.70%) rank (a); anthracite 857 ($R_{o,r}$ = = 4.14%) (b)

Рис. 3. Типичные диаграммы «нагружение–глубина внедрения», полученные при квази-статическом нано-индентировании углей разных стадий метаморфизма: каменный уголь низкой ($R_{o,r}$ = 0.56%), средней ($R_{o,r}$ = = 1.11%) и высокой ($R_{o,r}$ = 1.70%) стадии метаморфизма (а); антрацит 857 ($R_{o,r}$ = 4.14%) (б)

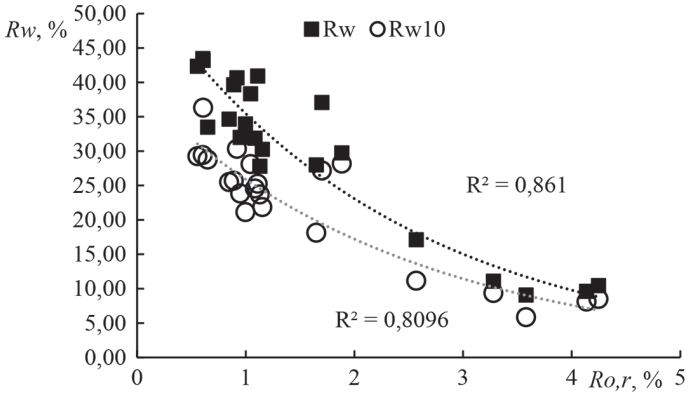

Fig. 4. Dependence of coals damage indices on rank

Рис. 4. Изменение показателя нарушенности углей в ряду метаморфизма

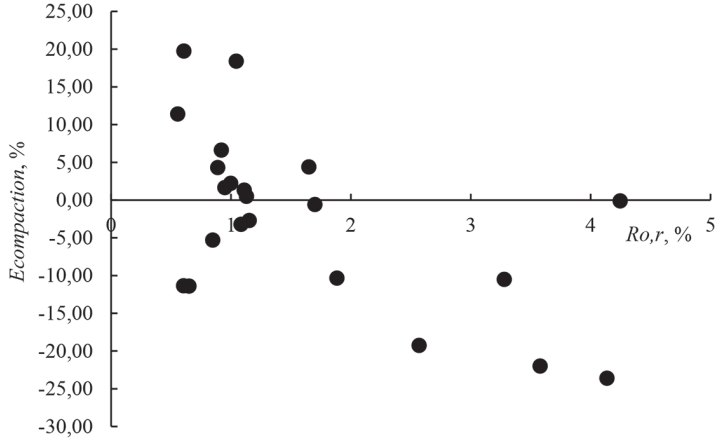

Fig. 5. Collation of coals' rank and compaction index

Рис. 5. Сопоставление стадии метаморфизма углей и показателя уплотнения

(see Fig. 4). It well correlates with the observations demonstrated in Fig. 3. It indicates on coals structure alteration connected with its compaction [33].

The obtained results indicate on the fact that there exists no correlation between $E_{compaction}$ values and coal rank (see Fig. 5). E.g., for anthracites 857 and 871 with close values of the reflection index (4.14 and 4.24%, respectively), $E_{compaction}$ varies from −23.61 to −0.12. This is consistent with previously obtained data [24].

It is noted that, for coals ##4, 1, 2, 10, 823, 825, 826, 827, 857 and 873, $E_{compaction}$ values are negative, for coals ##580, 581, 516, 824, 828, 829 they are positive, for coals ##517, 518, 822, 830, 839 and 871

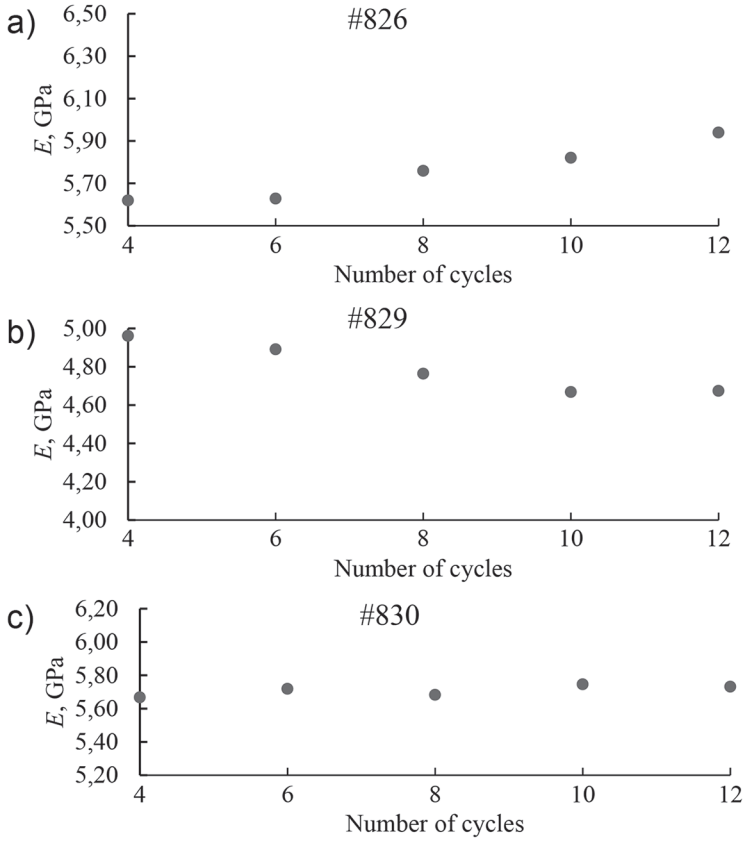

Fig. 6. Examples of changes in elastic moduli (stiffness) of coals during cyclic nanoindentation with increasing peak load. Three types of crushing mode are represented: 'local' mode with increase in stiffness of the matter (presumably due to formation of a core of crushed matter – 'powder' that is not allowing further destruction under the indenter) (a); 'bulk' mode – descend of stiffness (presumably due to disintegration of coal matter both inside the contact zone and outside it) (b); 'transition zone' – no alteration of stiffness is observed at each loading cycle (c)

Рис. 6. Примеры изменения величин модулей упругости (жесткости) углей при циклическом наноиндентировании с увеличивающейся нагрузкой. Представлены три типа по характеру разрушения: «локальное разрушение» — сопровождается увеличением жесткости (предположительно ввиду формирования ядра раскрошившегося материала («пудры»), препятствующего дальнейшему разрушению под воздействием индентора) (а); «разрушение в объеме» — плавное уменьшение жесткости (предположительно ввиду разрушения угольного вещества как в зоне контакта с индентором, так и вне ее) (б); «переходный тип» — при каждом последующем цикле нагружения не выявлено изменения жесткости угольного вещества (в)

they are close to zero. Thus, in the view of data described in [24], those coals having with negative $E_{compaction}$ are being crushed locally (in the contact zone with the indenter) during cyclic nanoindentation, with compaction of the formed fine particles, which leads to an increase in their locally measured stiffness (*E10*). Those with positive $E_{compaction}$ are being crushed in bulk (outside the zone of contact with the indenter).

Coals ##517, 518 822, 830, 839 and anthracite 871, due to no alteration of their stiffness after cyclic loading, here could be considered as being located in the transition region, and the features of their destruction mode should be studied further.

The following Fig. 6 demonstrates the alteration of coals elastic moduli values from cycle to cycle with reference to the typical behavior of representatives of different groups.

The nature of coals division into two branches in accordance with $E_{compaction}$ parameter could be described by the features of vitrinite organic matter structure [24]. The latter have been investigated by Raman spectroscopy and the parameter *S* was calculated in accordance with the scheme described in [24] and section 2.3 of the current paper (see eq.(4)). Note that is *S* index is greater than 1, then amorphous carbon predominates, if it is less than 1, then crystalline carbon predominates. The results of calculation are shown in Table 5. Some correlation between $E_{compaction}$ and *S* index are given in Fig. 7.

As can be seen from Fig. 7, there is a proportional relationship between $E_{compaction}$ and the ratio of amorphous and crystalline carbon compounds (*S*) in vitrinite. In this case, the transition from one crushing mode ('local') to a 'bulk' one occurs at the point when *S* = 1.

Thus, it can be assumed that the mode of coals crushing is determined by the ratio of the fractions of crystalline and amorphous carbon in vitrinite. The boundary of the transition from one type of crushing mode to another is an equal ratio of the shares of crystalline and amorphous carbon (*S* = 1). The studied coals attributed to the

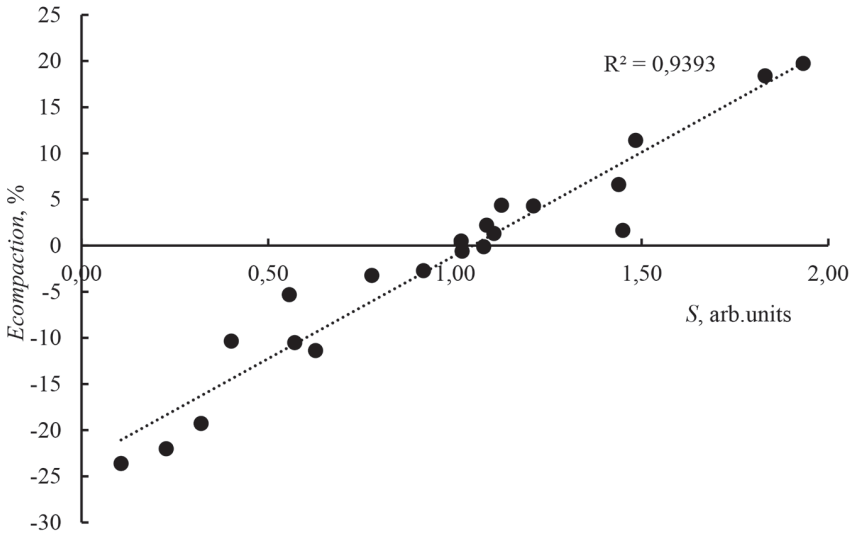

Fig. 7. The relationship between the mode of crushing of coals during cyclic nanoindentation and amorphous-to-crystalline carbon ratio in vitrinite

Рис. 7. Взаимосвязи между типом по характеру разрушения угольного вещества при циклическом наноиндентировании и соотношением аморфного и кристаллитного углерода в витрините углей

Table 5

Results of coals' vitrinites Raman spectra deconvolution in accordance with data on peaks characteristics (Table 3)
Результаты деконволюции Рамановских спектров в соответствии со схемой, представленной в табл. 3

Coal #	SL		D		VR		VL		GR		G		G2		S, arb. units
	position, cm^{-1}	area	position, cm^{-1}	area	position, cm^{-1}	area	position, cm^{-1}	area	position, cm^{-1}	area	position, cm^{-1}	area	position, cm^{-1}	area	
4*	1274	14 330	1350	29 601	–	–	1442	9912	1548	8823	1582	9040	1609	6487	0.733
580	1252	22 184	1331	30 250	1371	7657	1433	22 044	1551	12 922	1583	13 023	1609	10 277	1.210
581	1234	18 502	1311	29 069	1362	32 098	1440	20 267	1551	15 448	1582	17 364	1609	13 565	1.439
518	1239	4159	1322	10 172	1368	13 364	1482	4120	1560	4711	1587	4550	1611	3460	1.449
517	1247	8008	1324	12 117	1369	8435	1434	5515	1507	3212	1571	7470	1604	5169	1.017
516	1245	8887	1325	11 237	1368	6674	1431	6782	1512	3415	1573	6599	1604	5065	1.125
1	1236	3987	1331	20 369	1368	1501	–	–	1568	8266	1589	13 042	1607	9549	0.320
2	1248	11 735	1326	12 778	1368	6041	–	–	1551	6476	1585	15 989	1605	13 719	0.571
10	1213	17 212	1324	223 566	1365	31 127	–	–	1509	25 088	1575	55 109	1600	44 995	0.227
822	1248	27 691	1311	31 217	–	–	1443	13 917	1560	15 334	1591	12 822	1616	7511	1.105
823	1292	21 408	1358	53 769	–	–	1484	13 661	–	–	1571	18 998	1603	14 660	0.401
824	1254	7134	1316	17 044	1367	22 019	1454	9525	1554	13 326	1587	11 289	1614	6712	1.484
825	1250	20 168	1366	28 619	–	–	1455	11 109	1555	12 745	1588	12 192	1614	7263	0.916
826	1235	13 735	1347	43 301	1353	3540	1485	12 977	1568	14 504	1602	13 428	1642	830	0.778
827	1266	5970	1339	33 042	–	–	1422	12 640	1553	11 559	1586	9509	1612	5581	0.627
828	1244	8259	1309	17 088	1364	30 190	1455	11 752	1561	13 158	1591	11 071	1616	6451	1.831
829	1234	6480	1309	15 633	1351	30 250	1451	14 045	1555	12 519	1586	10 865	1614	6251	1.933
830	1299	37 035	1362	41 009	–	–	1454	19 014	1558	20 062	1589	17 296	1616	11 845	1.085
857	1212	13 644	1332	302 908	–	–	–	–	1520	27 556	1574	52 568	1603	33 640	0.106
839	1269	3453	1357	13 261	1355	6964	1460	11 115	1562	15 699	1592	11 868	1618	11 399	1.019
871	1215	20 913	1317	81 718	1355	58 278	1510	16 931	1573	22 092	1596	18 070	1616	9969	1.077
873	1268	42 721	1366	93 092	–	–	–	–	1528	31 820	1577	24 978	1611	15 878	0.556

* Italic font denotes coals that have been used in paper [24].

'transition zone' group (##517, 518, 822, 830, 839 and 871) are characterized by almost equal shares of crystalline and amorphous carbon compounds in their vitrinites.

The following summarizes the observations made. There exist two principal modes of coal vitrinite destruction under mechanical effects. Some coals tend to destroy locally in the contact zone (in our case — with the indenter), whereas some of them are being crushed in bulk. These modes are primarily predetermined by the vitrinite structural features, namely, the ratio of amorphous to crystalline carbon. If the crystalline carbon predominates, then the crushing mode is 'local', and the crushed zone serves as a preserver of the rest matter from crushing. This leads to 'increase' of stiffness of the material and the introduced parameter $E_{compaction}$ becomes negative. If the amorphous carbon predominates, then coal vitrinite is being crushed in bulk (i.e. including outside the contact zone with the indenter). In this case, the stiffness of the vitrinite descend during repeating mechanical influences, that results for $E_{compaction}$ being positive. Also, there exist hard coals and even anthracite whose vitrinite stiffness is not being altered during cyclic nanoindentation with increasing peak load. They are characterized by an even share of amorphous and crystalline carbon and are referred to a 'transition zone' between the crushing modes.

Conclusions

The results have been obtained that are in a good agreement with the known data of other authors on the fact that, in general, coal vitrinite strength increases with rank. In the context of the current study, the latter is indicated by the growth of stiffness (elastic moduli) and descend of the damage indices measured by the means of nanoindentation technique. It has been noted that such a variation of coals strength with rank is consistent for the repeatable mechanical effects implemented by the means of cyclic nanoindentation with increasing peak load.

A parameter $E_{compaction}$ has been introduced for characterization of the degree of alteration of vitrinite mechanical properties after the repeatable impacts (cyclic nanoindentation). It is calculated using the values of elastic moduli measured by quasi-static and cyclic nanoindentation after the tenth cycle of loading. The parameter $E_{compaction}$ reflects the mode of vitrinite crushing under cyclic mechanical effects and does not depend on rank for the selected range of coals. The studied coals were divided into three groups. For those coals whose $E_{compaction}$ is negative, the crushing mode is 'local' (only in the contact zone). For those coals, whose $E_{compaction}$ is positive, the crushing mode is 'bulk' (i.e. destruction of vitrinite matter is observed outside the contact zone). Three hard coals and one of the anthracites demonstrated almost no alteration of their stiffness during cyclic nanoindentation ($E_{compaction}$ is close to zero) and were attributed to the 'transition zone' between the two modes of crushing.

The mode of coal crushing under cyclic loading is strongly dependent on the vitrinite's structure characterized by Raman spectroscopy. The ratio of amorphous to crystalline carbon compounds in vitrinites (S) determines the values of $E_{compaction}$ parameter by linear trend. Moreover, the 'switching' between the crushing modes of coals during cyclic nanoindentation occurs when S reaches 1 sharp.

Coals with the 'local' crushing mode are characterized by crystalline carbon predomination in vitrinite matter. Coals with the 'bulk' crushing mode are those with amorphous carbon predomination in vitrinite. Coals from the 'transition zone' have been characterized by equal share of amorphous and crystalline carbon in their vitrinites.

СПИСОК ЛИТЕРАТУРЫ

1. *Trechera P., Moreno T., Córdoba P., Moreno N., Zhuang X., Li B., Li J., Shangguan Y., Dominguez A. O., Kelly F., Querol X.* Comprehensive evaluation of potential coal mine dust emissions in an open-pit coal mine in Northwest China // International Journal of Coal Geology. 2021, vol. 235, article 103677. DOI: 10.1016/J.COAL.2021.103677.

2. *Fabiano B., Currò F., Reverberi A. P., Palazzi E.* Coal dust emissions: From environmental control to risk minimization by underground transport. An applicative case-study // Process Safety and Environmental Protection. 2014, vol. 92, no. 2, pp. 150 — 159. DOI: 10.1016/j.psep.2013.01.002.

3. *Liu T., Liu S.* The impacts of coal dust on miners' health: A review // Environmental Research. 2020, vol. 190, article 109849. DOI: 10.1016/j.envres.2020.109849.

4. *Zhang R., Liu S., Zheng S.* Characterization of nano-to-micron sized respirable coal dust: Particle surface alteration and the health impact // Journal of Hazardous Materials. 2021, vol. 413, article 125447. DOI: 10.1016/j.jhazmat.2021.125447.

5. *Moreno T., Trechera P., Querol X., Lah R., Johnson D., Wrana A., Williamson B.* Trace element fractionation between PM10 and PM2.5 in coal mine dust: Implications for occupational respiratory health // International Journal of Coal Geology. 2019, vol. 203, pp. 52 — 59. DOI: 10.1016/j.coal.2019.01.006.

6. *Cai P., Nie W., Chen D., Yang S., Liu Z.* Effect of air flowrate on pollutant dispersion pattern of coal dust particles at fully mechanized mining face based on numerical simulation // Fuel. 2019, vol. 239, pp. 623 — 635. DOI: 10.1016/j.fuel.2018.11.030.

7. *Li Q., Wang K., Zheng Y., Ruan M., Mei X., Lin B.* Experimental research of particle size and size dispersity on the explosibility characteristics of coal dust // Powder Technology. 2016, vol. 292, pp. 290 — 297. DOI: 10.1016/j.powtec.2016.01.035.

8. *Panov G. E.* Dust formation kinetics as a function of the principal mechanical properties of coals // Soviet Mining Science. 1967, vol. 3, no. 5, pp. 511 — 514. DOI: 10.1007/BF02497948.

9. *Zipf R. K., Bieniawski Z. T.* Estimating the crush zone size under a cutting tool in coal // International Journal of Mining and Geological Engineering. 1988, vol. 6, no. 4, pp. 279 — 295. DOI: 10.1007/BF00880927.

10. *Baafi E. Y., Ramani R. V.* Rank and maceral effects on coal dust generation // International Journal of Rock Mechanics and Mining Sciences & Geomechanics Abstracts. 1979, vol. 16, no. 2, pp. 107 — 115. DOI: 10.1016/0148-9062(79)91447-5.

11. *Hower J. C., Graese A. M., Klapheke J. G.* Influence of microlithotype composition on hardgrove grindability for selected eastern Kentucky coals // International Journal of Coal Geology. 1987, vol. 7, no. 3, pp. 227 — 244. DOI: 10.1016/0166-5162(87)90038-3.

12. *Organiscak J. A., Page S. J.* Laboratory investigation of coal grindability and airborne respirable dust // Journal of the Mine Ventilation Society of South Africa. 1993, vol. 46, no. 7, pp. 98 — 105.

13. *Hower J. C.* Interrelationship of coal grinding properties and coal petrology // Minerals and Metallurgical Processing. 1998, vol. 15, no. 3, pp. 1 — 16. DOI: 10.1007/BF03403218.

14. *Page S. J., Organiscak J. A.* Using proximate analysis to characterize airborne dust generation from bituminous coals // Aerosol Science and Technology. 2002, vol. 36, no. 6, pp. 721 — 733. DOI: 10.1080/02786820290038393.

15. *Bagherieh A. H., Hower J. C., Bagherieh A. R.*, Jorjani E. Studies of the relationship between petrography and grindability for Kentucky coals using artificial neural network // International Journal of Coal Geology. 2008, vol. 73, no. 2, pp. 130 — 138. DOI: 10.1016/j.coal.2007.04.002.

16. *Organiscak J. A., Page S. J.* Airborne dust liberation during coal crushing // Coal Preparation. 2000, vol. 21, no. 5-6, pp. 423 — 453. DOI: 10.1080/07349340108945630.

17. *Page S. J., Organiscak J. A., Quattro J.* Coal proximate analyses correlation with airborne respirable dust // Fuel. 1993, vol. 72, no. 7, pp. 965 — 970. DOI: 10.1016/0016-2361(93)90293-B.

18. *Page S. J.*, *Organiscak J. A.* Suggestion of a cause-and-effect relationship among coal rank, airborne dust, and incidence of workers' pneumoconiosis // Aihaj. 2000, vol. 61, no. 6, pp. 785 — 787.

19. *Kossovich E. L.*, *Borodich F. M.*, *Epshtein S. A.*, *Galanov B. A.*, *Minin M. G.*, *Prosina V. A.* Mechanical, structural and scaling properties of coals: depth-sensing indentation studies // Applied Physics A. 2019, vol. 125, no. 3, pp. 195. DOI: 10.1007/s00339-018-2282-1.

20. *Ren Q., Zhang Y., Arauzo I., Shan L., Xu J., Wang Y., Su S., Hu S., Xiang J.* Roles of moisture and cyclic loading in microstructures and their effects on mechanical properties for typical Chinese bituminous coals // Fuel. 2021, vol. 293, pp. 120408. DOI: 10.1016/j.fuel.2021.120408.

21. *Zhou W., Wang H., Wang D., Du Y., Zhang K., Kang W.* The effect of coal proximate compositions on the characteristics of dust generation using a conical pick cutting system // Powder Technology. 2019, vol. 355, pp. 573 — 581. DOI: 10.1016/j.powtec.2019.07.093.

22. *Argatov I. I.*, *Borodich F. M.*, *Epshtein S. A.*, *Kossovich E. L.* Contact stiffness depth-sensing indentation: Understanding of material properties of thin films attached to substrates // Mechanics of Materials. 2017, vol. 114, pp. 172 — 179. DOI: 10.1016/j.mechmat.2017.08.009.

23. *Агарков К. В.*, *Эпштейн С. А.*, *Коссович Е. Л.*, *Добрякова Н. Н.* Исследование низкотемпературных воздействий на механические свойства углей на микроуровне и склонность к образованию аэрозольной пыли // Горный журнал. — 2022. — № 4. — С. 66 — 72. DOI: 10.17580/gzh.2022.04.11.

24. *Kossovich E. L.*, *Epshtein S. A.*, *Krasilova V. A.*, *Hao J.*, *Minin M. G.* Effects of coals microscale structural features on their mechanical properties, propensity to crushing and fine dust formation // International Journal of Coal Science and Technology. 2022, in Press.

25. *Коссович Е. Л.*, *Добрякова Н. Н.*, *Эпштейн С. А.*, *Белов Д. С.* Определение механических свойств микрокомпонентов углей методом непрерывного индентирования // Физико-технические проблемы разработки полезных ископаемых. — 2016. — № 5. — С. 84 — 91.

26. *Bulychev S. I.*, *Alekhin V. P.*, *Shorshorov M. K.*, *Ternovskij A. P.*, *Shnyrev G. D.* Determination of Young modulus by the hardness indentation diagram // Zavodskaya Laboratoriya. 1975, vol. 41, no. 9, pp. 1137 — 1140.

27. *Коссович Е. Л.*, *Эпштейн С. А.*, *Добрякова Н. Н.*, *Минин М. Г.* Структурные особенности и механические свойства антрацита, метаантрацита и графита // Горный журнал. — 2020. — № 4. — С. 25 — 29. DOI: 10.17580/gzh.2020.04.05.

28. *Коссович Е. Л.*, *Эпштейн С. А.*, *Голубева М. Д.*, *Красилова В. А.* Разработка методики циклического наноиндентирования для оценки склонности углей к образованию пыли // Горный информационно-аналитический бюллетень. — 2021. — № 5. — С. 112 — 121. DOI: 10.25018/0236_1493_2021_5_0_112.

29. *Коссович Е. Л.*, *Эпштейн С. А.*, *Бородич Ф. М.*, *Добрякова Н. Н.*, *Просина В. А.* Взаимосвязи между неоднородностью распределения механических свойств углей на микро- и наноуровнях и их способностью к внезапным выбросам и разрушению // Горный информационно-аналитический бюллетень. — 2019. — № 5. — С. 156 — 172. DOI: 10.25018/02361493-2019-05-0-156-172.

30. *Sadezky A., Muckenhuber H., Grothe H., Niessner R., Pöschl U.* Raman microspectroscopy of soot and related carbonaceous materials: Spectral analysis and structural information // Carbon. 2005, vol. 43, no. 8, pp. 1731 — 1742. DOI: 10.1016/j.carbon.2005.02.018.

31. *Ulyanova E. V.*, *Molchanov A. N.*, *Prokhorov I. Y.*, *Grinyov V. G.* Fine structure of Raman spectra in coals of different rank // International Journal of Coal Geology. 2014, vol. 121, pp. 37 — 43. DOI: 10.1016/j.coal.2013.10.014.

32. *Xu J., Tang H., Su S., Liu J., Xu K., Qian K., Wang Y., Zhou Y., Hu S., Zhang A., Xiang J.* A study of the relationships between coal structures and combustion characteristics: The insights from micro-Raman spectroscopy based on 32 kinds of Chinese coals // Applied Energy. 2018, vol. 212, pp. 46 — 56. DOI: 10.1016/j.apenergy.2017.11.094.

33. *Hirsch P. B.* X-Ray scattering from coals // Proceedings of the Royal Society A: Mathematical, Physical and Engineering Sciences. 1954, vol. 226, no. 1165, pp. 143—169. DOI: 10.1098/rspa.1954.0245. ГИАБ

REFERENCES

1. Trechera P., Moreno T., Córdoba P., Moreno N., Zhuang X., Li B., Li J., Shangguan Y., Dominguez A. O., Kelly F., Querol X. Comprehensive evaluation of potential coal mine dust emissions in an open-pit coal mine in Northwest China. *International Journal of Coal Geology*. 2021, vol. 235, article 103677. DOI: 10.1016/J.COAL.2021.103677.

2. Fabiano B., Currò F., Reverberi A. P., Palazzi E. Coal dust emissions: From environmental control to risk minimization by underground transport. An applicative case-study. *Process Safety and Environmental Protection*. 2014, vol. 92, no. 2, pp. 150—159. DOI: 10.1016/j.psep.2013.01.002.

3. Liu T., Liu S. The impacts of coal dust on miners' health: A review. *Environmental Research*. 2020, vol. 190, article 109849. DOI: 10.1016/j.envres.2020.109849.

4. Zhang R., Liu S., Zheng S. Characterization of nano-to-micron sized respirable coal dust: Particle surface alteration and the health impact. *Journal of Hazardous Materials*. 2021, vol. 413, article 125447. DOI: 10.1016/j.jhazmat.2021.125447.

5. Moreno T., Trechera P., Querol X., Lah R., Johnson D., Wrana A., Williamson B. Trace element fractionation between PM10 and PM2.5 in coal mine dust: Implications for occupational respiratory health. *International Journal of Coal Geology*. 2019, vol. 203, pp. 52—59. DOI: 10.1016/j.coal.2019.01.006.

6. Cai P., Nie W., Chen D., Yang S., Liu Z. Effect of air flowrate on pollutant dispersion pattern of coal dust particles at fully mechanized mining face based on numerical simulation. *Fuel*. 2019, vol. 239, pp. 623—635. DOI: 10.1016/j.fuel.2018.11.030.

7. Li Q., Wang K., Zheng Y., Ruan M., Mei X., Lin B. Experimental research of particle size and size dispersity on the explosibility characteristics of coal dust. *Powder Technology*. 2016, vol. 292, pp. 290—297. DOI: 10.1016/j.powtec.2016.01.035.

8. Panov G. E. Dust formation kinetics as a function of the principal mechanical properties of coals. *Soviet Mining Science*. 1967, vol. 3, no. 5, pp. 511—514. DOI: 10.1007/BF02497948.

9. Zipf R. K., Bieniawski Z. T. Estimating the crush zone size under a cutting tool in coal. *International Journal of Mining and Geological Engineering*. 1988, vol. 6, no. 4, pp. 279—295. DOI: 10.1007/BF00880927.

10. Baafi E. Y., Ramani R. V. Rank and maceral effects on coal dust generation. *International Journal of Rock Mechanics and Mining Sciences & Geomechanics Abstracts*. 1979, vol. 16, no. 2, pp. 107—115. DOI: 10.1016/0148-9062(79)91447-5.

11. Hower J. C., Graese A. M., Klapheke J. G. Influence of microlithotype composition on hardgrove grindability for selected eastern Kentucky coals. *International Journal of Coal Geology*. 1987, vol. 7, no. 3, pp. 227—244. DOI: 10.1016/0166-5162(87)90038-3.

12. Organiscak J. A., Page S. J. Laboratory investigation of coal grindability and airborne respirable dust. *Journal of the Mine Ventilation Society of South Africa*. 1993, vol. 46, no. 7, pp. 98—105.

13. Hower J. C. Interrelationship of coal grinding properties and coal petrology. *Minerals and Metallurgical Processing*. 1998, vol. 15, no. 3, pp. 1—16. DOI: 10.1007/BF03403218.

14. Page S. J., Organiscak J. A. Using proximate analysis to characterize airborne dust generation from bituminous coals. *Aerosol Science and Technology*. 2002, vol. 36, no. 6, pp. 721—733. DOI: 10.1080/02786820290038393.

15. Bagherieh A. H., Hower J. C., Bagherieh A. R., Jorjani E. Studies of the relationship between petrography and grindability for Kentucky coals using artificial neural network. *Inter-*

national Journal of Coal Geology. 2008, vol. 73, no. 2, pp. 130 – 138. DOI: 10.1016/j.coal.2007.04.002.

16. Organiscak J. A., Page S. J. Airborne dust liberation during coal crushing. *Coal Preparation*. 2000, vol. 21, no. 5-6, pp. 423 – 453. DOI: 10.1080/07349340108945630.

17. Page S. J., Organiscak J. A., Quattro J. Coal proximate analyses correlation with airborne respirable dust. *Fuel*. 1993, vol. 72, no. 7, pp. 965 – 970. DOI: 10.1016/0016-2361(93)90293-B.

18. Page S. J., Organiscak J. A. Suggestion of a cause-and-effect relationship among coal rank, airborne dust, and incidence of workers' pneumoconiosis. *Aihaj*. 2000, vol. 61, no. 6, pp. 785 – 787.

19. Kossovich E. L., Borodich F. M., Epshtein S. A., Galanov B. A., Minin M. G., Prosina V. A. Mechanical, structural and scaling properties of coals: depth-sensing indentation studies. *Applied Physics A*. 2019, vol. 125, no. 3, pp. 195. DOI: 10.1007/s00339-018-2282-1.

20. Ren Q., Zhang Y., Arauzo I., Shan L., Xu J., Wang Y., Su S., Hu S., Xiang J. Roles of moisture and cyclic loading in microstructures and their effects on mechanical properties for typical Chinese bituminous coals. *Fuel*. 2021, vol. 293, pp. 120408. DOI: 10.1016/j.fuel.2021.120408.

21. Zhou W., Wang H., Wang D., Du Y., Zhang K., Kang W. The effect of coal proximate compositions on the characteristics of dust generation using a conical pick cutting system. *Powder Technology*. 2019, vol. 355, pp. 573 – 581. DOI: 10.1016/j.powtec.2019.07.093.

22. Argatov I. I., Borodich F. M., Epshtein S. A., Kossovich E. L. Contact stiffness depth-sensing indentation: Understanding of material properties of thin films attached to substrates. *Mechanics of Materials*. 2017, vol. 114, pp. 172 – 179. DOI: 10.1016/j.mechmat.2017.08.009.

23. Agarkov K. V., Epstein S. A., Kossovich E. L., Dobryakova N. N. Effects of low-temperature treatment on the coals mechanical properties microscale and airborne dust formation. *Gornyi Zhurnal*. 2022, no. 4, pp. 66 – 72. [In Russ]. DOI: 10.17580/gzh.2022.04.11.

24. Kossovich E. L., Epshtein S. A., Krasilova V. A., Hao J., Minin M. G. Effects of coals microscale structural features on their mechanical properties, propensity to crushing and fine dust formation. *International Journal of Coal Science and Technology*. 2022, in Press.

25. Kossovich E. L., Dobryakova N. N., Epshtein S. A., Belov D. S. Mechanical properties of coal microcomponents under continuous indentation. *Fiziko-tekhnicheskiye problemy razrabotki poleznykh iskopayemykh*. 2016, no. 5, pp. 84 – 91. [In Russ].

26. Bulychev S. I., Alekhin V. P., Shorshorov M. K., Ternovskij A. P., Shnyrev G. D. Determination of Young modulus by the hardness indentation diagram. *Zavodskaya Laboratoriya*. 1975, vol. 41, no. 9, pp. 1137 – 1140.

27. Kossovich E. L., Epshtein S. A., Dobryakova N. N., Minin M. G. Structural features and mechanical properties of anthracite, metaanthracite and graphite. *Gornyi Zhurnal*. 2020, no. 4, pp. 25 – 29. [In Russ]. DOI: 10.17580/gzh.2020.04.05.

28. Kossovich E. L., Epshtein S. A., Golubeva M. D., Krasilova V. A. On using cyclic nanoindentation technique to assess coals propensity to fine dust formation. *MIAB. Mining Inf. Anal. Bull.* 2021, no. 5, pp. 112 – 121. [In Russ]. DOI: 10.25018/0236_1493_2021_5_0_112.

29. Kossovich E. L., Epshtein S. A., Borodich F. M., Dobryakova N. N., Prosina V. A. Connections between micro/nano scale heterogeneity of mechanical properties of coals and their propensity to outbursts and crushing. *MIAB. Mining Inf. Anal. Bull.* 2019, no. 5, pp. 156 – 172. [In Russ]. DOI: 10.25018/02361493-2019-05-0-156-172.

30. Sadezky A., Muckenhuber H., Grothe H., Niessner R., Pöschl U. Raman microspectroscopy of soot and related carbonaceous materials: Spectral analysis and structural information. *Carbon*. 2005, vol. 43, no. 8, pp. 1731 – 1742. DOI: 10.1016/j.carbon.2005.02.018.

31. Ulyanova E. V., Molchanov A. N., Prokhorov I. Y., Grinyov V. G. Fine structure of Raman spectra in coals of different rank. *International Journal of Coal Geology*. 2014, vol. 121, pp. 37 – 43. DOI: 10.1016/j.coal.2013.10.014.

32. Xu J., Tang H., Su S., Liu J., Xu K., Qian K., Wang Y., Zhou Y., Hu S., Zhang A., Xiang J. A study of the relationships between coal structures and combustion characteristics: The insights from micro-Raman spectroscopy based on 32 kinds of Chinese coals. *Applied Energy*. 2018, vol. 212, pp. 46—56. DOI: 10.1016/j.apenergy.2017.11.094.

33. Hirsch P. B. X-Ray scattering from coals. *Proceedings of the Royal Society A: Mathematical, Physical and Engineering Sciences*. 1954, vol. 226, no. 1165, pp. 143—169. DOI: 10.1098/rspa.1954.0245.

ИНФОРМАЦИЯ ОБ АВТОРАХ

Эпштейн Светлана Абрамовна[1] — д-р техн. наук,
зав. лабораторией,
e-mail: apshtein@yandex.ru,
Коссович Елена Леонидовна[1] — канд. физ.-мат. наук,
старший научный сотрудник,
e-mail: e.kossovich@misis.ru,
Минин Максим Геннадьевич[1] — ведущий инженер
научного проекта,
Добрякова Надежда Николаевна[1] — канд. техн. наук,
научный сотрудник,
Гаврилова Дарья Ивановна[1] — канд. техн. наук,
[1] НУИЛ ФХУ, НИТУ «МИСиС».
Для контактов: Коссович Е.Л., e-mail: e.kossovich@misis.ru.

INFORMATION ABOUT THE AUTHORS

S.A. Epshtein[1], Dr. Sci. (Eng.),
Head of Laboratory,
e-mail: apshtein@yandex.ru,
E.L. Kossovich[1], Cand. Sci. (Phys. Mathem.),
Senior Researcher,
e-mail: e.kossovich@misis.ru,
M.G. Minin[1], Leading Engineer
of Scientific Project,
N.N. Dobryakova[1], Cand. Sci. (Eng.),
Researcher,
D.I. Gavrilova[1], Cand. Sci. (Eng.),
[1] NUIL FHU, National University of Science
and Technology «MISiS», 119049, Moscow, Russia.
Corresponding author: E.L. Kossovich, e-mail: e.kossovich@misis.ru.

Получена редакцией 16.12.2022; получена после рецензии 06.03.2023; принята к печати 10.03.2023.
Received by the editors 16.12.2022; received after the review 06.03.2023; accepted for printing 10.03.2023.